ENVIRONMENTAL ENGINEERING SCIENCE
Volume 00, Number 00, 2021

DOI: 10.1089/ees.2021.0160

Evaluation of Absolute Maximum Urban Heat Island Intensity Based on a Simplified Remote Sensing Approach

Valentino Sangiorgio,[1–3,*,i] Alessandra Capolupo,[1,ii] Eufemia Tarantino,[1] Francesco Fiorito,[1,3] and Mattheos Santamouris[4]

[1]*DICATECh, Polytechnic University of Bari, Bari, Italy.*
[2]*ICITECH, Polytechnic University of Valencia, València, Spain.*
[3]*FEUP—University of Porto, Porto, Portugal.*
[4]*High Performance Architecture, School of Built Environment, University of New South Wales, Sydney, Australia.*

Received: April 13, 2021 *Accepted in revised form: July 15, 2021*

Abstract

The Urban Heat Island (UHI) phenomenon can be harmful during the summer season jeopardizing the safety of some vulnerable population classes. Typically, the study of the UHI requires long data acquisitions using weather stations widely distributed within the cities. To this aim, recent research proposed multicriteria approaches aimed at quantifying the hazard of the summer absolute maximum Urban Heat Island Intensity (UHII), in urban districts. On the contrary, these approaches are time consuming and involve a large number of parameters. This article proposes a simplified multiparametric approach based on the three principal parameters involved in the UHI (*albedo*, *greenery*, and *anthropogenic heat*) obtained by a refined remote sensing data acquisition. In comparison with other approaches, the proposed method is simpler and quick to apply while maintaining good precision. Moreover, a calibration is achieved by exploiting the real absolute max UHII of a set of 41 European urban districts and a validation is obtained by a comparison with another multiparametric approach already validated in literature. Both the approaches are applied to 96 urban districts of Berlin. The results show that the simplified procedure keep an average error less than 1°C but improving in applicability.

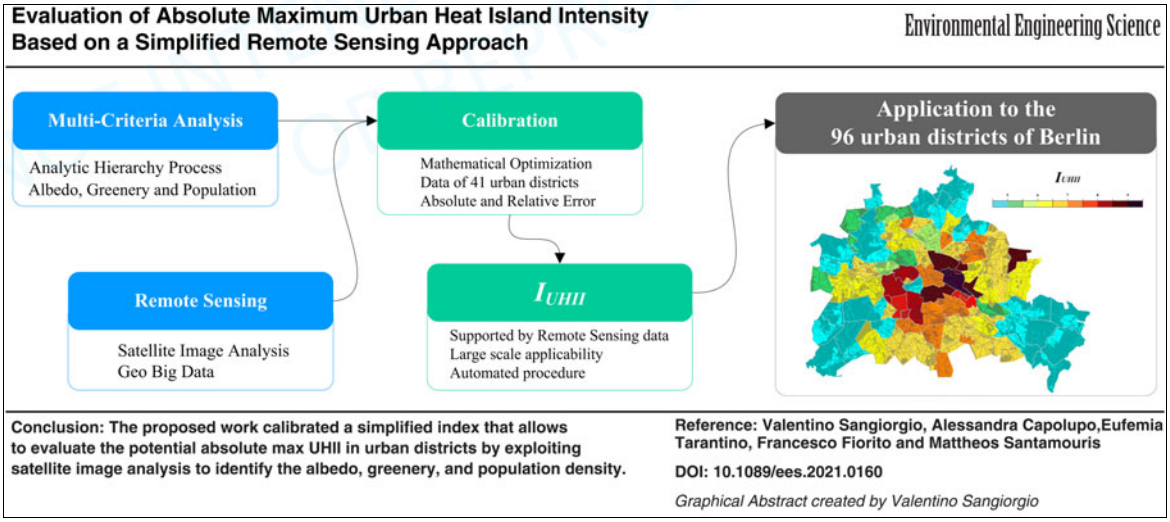

Keywords: Building Stock; Google Earth Engine; greenery; Index Calibration; satellite image analysis; Urban Heat Island; Urban Surface Materials

**Corresponding author:* DICATECh, Polytechnic University of Bari, Via Edoardo Orabona 4, Bari 70126, Italy. *Phone:* +34 656469784; *E-mail:* valentino.sangiorgio@poliba.it
[i]ORCID ID (https://orcid.org/0000-0002-7534-3177).
[ii]ORCID ID (https://orcid.org/0000-0002-4103-1992).

Introduction

Over the past decades, global warming has been in the spotlight since it is threatening human well-being and environment health (McMichael *et al.*, 2006; Singh and Purohit, 2014). However, just in the past few years, it has been noted that overheating consequences can be exacerbated or mitigated by human activities (Weng *et al.*, 2004; Al-Ghussain, 2019). Indeed, it has been amply demonstrated that anthropogenic actions altered natural land covers that directly affects the albedo, heat conductivity, and moisture of a specific zone (Apollonio *et al.*, 2016; Capolupo *et al.*, 2018; Boccia *et al.*, 2020), causing the increment or the decrement of air and surface temperatures in such area. Specifically, the phenomenon of the Urban Heat Island (UHI), regarding higher air temperatures within urban districts compared with the surrounding rural environments, raised concern in the scientific world (Santamouris, 2020). In the related literature, the parameters influencing the Urban Heat Island Intensity (UHII) have been widely studied (Oke, 1991) and identified in the following: (1) meteorological variables; (2) urban morphological features; (3) building materials; (4) anthropogenic heat; and (5) city canyons. The detection of the main triggering factors and the prediction of the phenomenon are essential to identify the optimal strategies to be adopted to contrast their main effects on human well-being and comfort, such as the increase in mortality rate (Pantavou *et al.*, 2011) and cardiovascular illness (Heaviside *et al.*, 2016), and, to reduce cooling energy consumption during summertime (Santamouris, 2015).

Conventionally, to measure the UHII *in situ*, automatic weather stations are required (Oke *et al.*, 2017). Anyway, this information is not always available because weather stations are patchy distributed within the cities and, consequently, large areas may be without coverage. To overcome this constraint, numerical simulations-based approaches, which simultaneously include several parameters (e.g., meteorological data, urban surface characteristics, and climate conditions), may be adopted. Nevertheless, also numerical simulations have limitations because the numerous input parameters of the models need to be measured or estimated (Cantelli *et al.*, 2015).

To this aim, a recent research proposed a new multiparametric index I_{UHII} aimed at quantifying the hazard of the absolute maximum UHII in urban districts during the summer season by taking into account all the parameters influencing the phenomenon based on open-source data (Sangiorgio *et al.*, 2020). This I_{UHII} is based on 11 parameters including *meteorological variables*, *characteristics of the city*, *anthropogenic heat*, and *city canyons*. The advantage in comparison with the other approaches is the possibility to consider numerous qualitative and quantitative aspects in the analysis, involving a multicriteria-based procedure for the calibration. In this approach, fundamental parameters such as *albedo* and *greenery* are evaluated by an image analysis, which breaks down satellite image to individuate urban district materials (asphalt, water, white plaster, red brick, etc.) and presence of greenery. On the contrary, the existing index-based approaches are time consuming and based on manual and slow calculations.

A widely used effective and fast approach to extract *albedo* and *greenery* is offered by remote sensing (RS) techniques. In the related literature, RS tools have been recognized as the most effective instrument to compute the urban surface characteristics contributing to UHI phenomenon (Chen *et al.*, 2006; Mirzaei *et al.*, 2020). In recent years, specific algorithms have been defined to compute the albedo from each satellite mission (Caprioli and Tarantino, 2001; Tarantino and Figorito, 2012; Sarzana *et al.*, 2020). In addition, the use of RS techniques allows to overcome time-consuming analysis by processing a large amount of geospatial information and using cloud-based platforms handling geo-big data at large scale. Among them, Google Earth Engine (GEE), recently released by Google to process RS data, is a cloud free environment that enables parallelized processing of a huge amount of information belonging to various data sources (Gorelick *et al.*, 2017). In addition, its excellent computational power, owing to the application of many processors, minimizes sensed data processing time. Thus, GEE has strongly improved the RS world to evaluate albedo and greenery on a large scale.

This article proposes a simplified index to evaluate the absolute maximum UHII by combining the multicriteria approach (Sangiorgio *et al.*, 2020) with RS techniques to obtain a fast and easy procedure (Caprioli and Tarantino, 2001; Tarantino and Figorito, 2012; Sarzana *et al.*, 2020). The index is evaluated considering the three most important parameters in the UHII generation: *albedo*, *greenery*, and *anthropogenic heat*. The resulting approach allows large-scale data acquisition exploiting cloud-based platforms and large-scale geo-big data analysis to identify albedo and greenery in urban districts (Chen *et al.*, 2006; Wang *et al.*, 2008; Mirzaei *et al.*, 2020). In comparison with previous studies, the main novelty of such approach regards a significant increase in usefulness and applicability of the new index, thanks to the synergy of a multiparametric approach with geo-big data analysis (that allows examining 100 processors in parallel). In addition, the proposed index maintains high accuracy even if it is simplified in comparison with approaches that contemplate numerous parameters.

The article is organized as follows. Overview of the Methodological Approach to Achieve the Index section proposes an overview of the methodological approach and The Definition of the Index and Data Acquisition Process section presents the simplified index and the RS data acquisition procedure. Moreover, Calibration section shows the calibration of the Index and Application and Comparison section shows its application and comparison. Finally, Conclusions section draws conclusions of this research work.

Overview of the Methodological Approach to Achieve the Index

This research is achieved in two phases (Fig. 1): (1) the calibration of the proposed index; and (2) the application and validation of the index performed by comparison with the multiparametric index I_{UHII} of Sangiorgio *et al.* (2020).

In the first phase, the proposed index is calibrated. In this phase an analytic hierarchy process (AHP) is used to analyze and structure the problem in its basic components (macrocriteria, criteria, and intensity ranges) and define the index. Successively, data acquisition is performed to acquire *albedo*, *greenery*, and *anthropogenic heat* through an

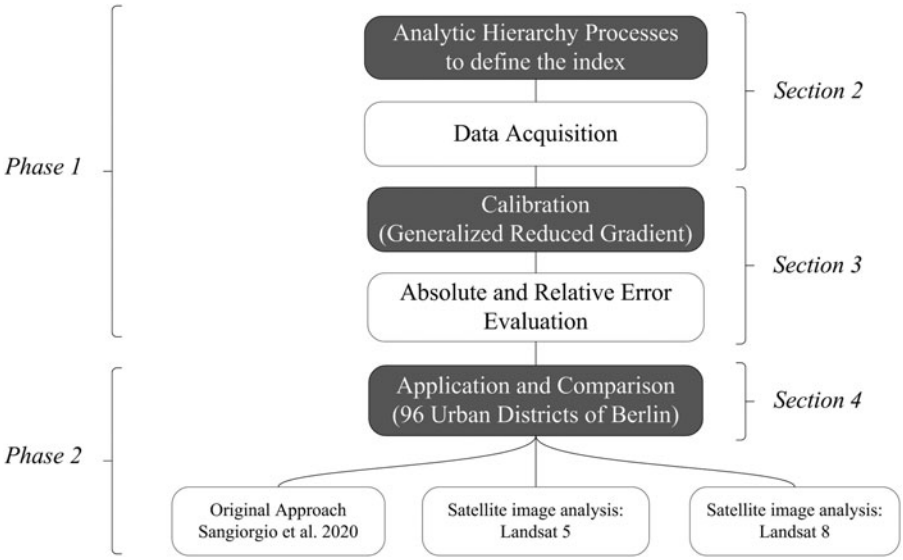

FIG. 1. The two phases of the proposed methodology to define, calibrate, and compare the proposed index.

RS approach. Once the dataset is realized, an optimization procedure (Sangiorgio *et al.*, 2019; Sangiorgio and Parisi, 2020) is used to calibrate the index exploiting the effective UHII data acquired in 41 urban districts of 32 different European cities (obtained from an exhaustive bibliographic analysis). In addition, the calibration exploits a Jackknife approach to perform a resampling of the input data and achieve a statistical graph of the absolute and relative error of the Index.

In the second phase, both the proposed simplified indices exploiting the RS tools and the multiparametric index of Sangiorgio *et al.* (2020) are applied to 96 urban districts of Berlin. A comparison is carried out by evaluating the differences of the forecasted absolute max UHII for every urban district using different approaches. In addition, the effectiveness of the proposed calibration is tested with both the satellite data from Landsat 5 and Landsat 8.

Definition of the Index and Data Acquisition Process

In this section, the index is defined and discussed using the AHP. In addition, the proposed data acquisition procedure to include RS tools in the index evaluation is described in detail. In particular, a specific focus in this work is dedicated to data acquisition of the *Characteristics of the City* in terms of *Albedo* and *Greenery* with a satellite image analysis.

The AHP to define the index

The proposed index is based on two *macrocriteria* and three *criteria i* (with $i=1,\ldots,3$) that are the principal parameters involved in the generation of the absolute max UHII (Sangiorgio *et al.*, 2020). For each *criterion*, a set of *intensity ranges j* (with $j=1, \ldots, n_i$) is defined to characterize its intensity levels. The three criteria and related intensity ranges are structured in a hierarchical flowchart as given in Fig. 2 and described in the following.

The first macrocriterion regards the *Characteristics of the City* in the UHII accounting the first and second criteria:

(1) *Land Cover Types* (*Albedo*) ($i=1$) including 10 intensity ranges ($n_1=10$);
(2) *Land Cover* (*Greenery*) ($i=2$) to consider the phenomenon of evapotranspiration through 10 ranges ($n_2=10$).

The other macrocriterion is the anthropogenic heat. The anthropogenic heat can be evaluated by considering the

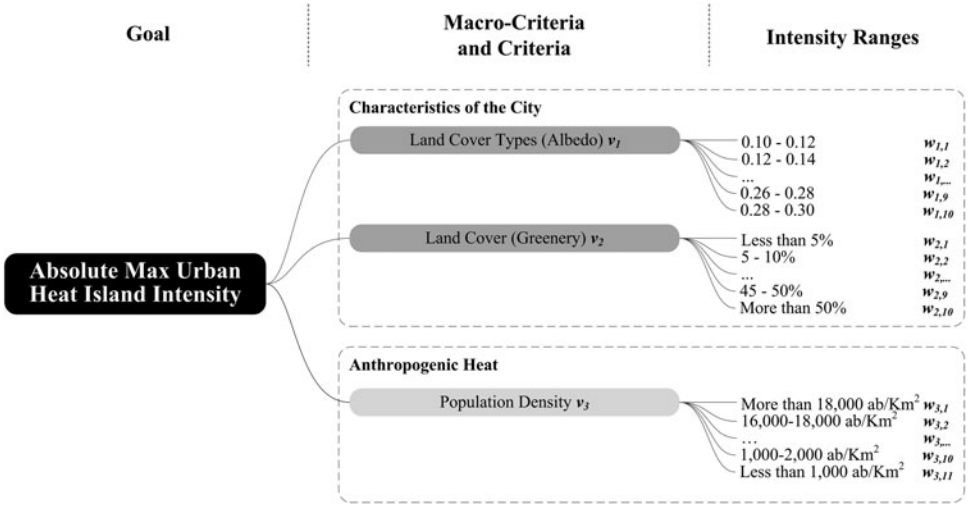

FIG. 2. Structure of the problem: weight criteria and intensity ranges to define the index able to quantify the potential absolute max UHII in urban district (Sangiorgio *et al.*, 2020). UHII, Urban Heat Island Intensity.

linear dependence between anthropogenic heat and population density according to Merkin (2004):

(3) *Population Density* ($i=3$) including 11 related ranges ($n_3=11$).

Once the criteria are defined, the simplified index ($\boldsymbol{I}_{\mathrm{RS,UHII}}$) to evaluate the potential absolute max UHII using RS data can be evaluated as follows:

$$\boldsymbol{I}_{\mathrm{RS,\,UHII}} = v_1 \times w_{1j} + v_2 \times w_{2j} + v_3 \times w_{3j} \quad (1)$$

where v_i and w_{ij} are the weights associated to the *criterion i* and to the *intensity ranges j*, respectively.

Note that the relation between every single intensity ranges and the associate weights w_{ij} in the UHII development have already been investigated in literature (Sangiorgio *et al.*, 2020). Such relation remains valid also for the proposed RS-based index because the obtained values of weights do not depend on the data acquisition procedure. The weights w_{ij} are given in Table 1.

However, the weight v_i representing the influence of every parameter in the phenomenon needs to be calibrated to get the simplified index.

Data acquisition

This section explains the process of data acquisition that is used for calibration in the Calibration section. To perform the calibration, this work exploits and reports the effective UHII data acquired for 41 urban districts of 35 different cities in the European continent.

In addition, *characteristics of the city* and *anthropogenic heat* data are extracted for the 41 investigated urban districts.

UHII extraction from bibliographic analysis. This study exploits published experimental data (acquired with fixed weather stations) on the max UHI magnitude of 35 different cities in 11 different countries of the European continent. The obtained data of specific urban districts, related geographic coordinates, and related UHII measured are given in Fig. 3. For every urban district, a specific identification code Ud = 1,…,41 is assigned. In particular, the acquired information is collected from 15 scientific articles published in peer review journals, books, and research reports as reported in the following: Russia (Varentsov *et al.*, 2018), the Netherlands (Van Hove *et al.*, 2011), Italy (Petralli *et al.*, 2006; Giovannini *et al.*, 2011; Busato *et al.*, 2014; Milelli, 2016; Guattari *et al.*, 2018; Marando *et al.*, 2019), United Kingdom (Kolokotroni and Giridharan, 2008), Spain (Santamouris, 2016), Scotland (Krüger and Emmanuel, 2013), Turkey (Tayanc and Toros, 1997), Romania (Cheval *et al.*, 2009) Poland (Fortuniak *et al.*, 2006), and France (Lemonsu and Masson, 2002).

Characteristics of the city—satellite image analysis approach. This subsection describes in detail the RS approach used to individuate data *albedo* and *greenery* in the

Table 1. Tabulated Weight Obtained by Applying Analytic Hierarchy Processes Step 2

Macrocriteria	*Criteria*	*Intensity ranges*	$w_{i,j}$	*Value*
Characteristics of the city	Land cover types (albedo)	0.10–0.12	$w_{1,1}$	1
		0.12–0.14	$w_{1,2}$	0.85
		0.14–0.16	$w_{1,3}$	0.73
		0.16–0.18	$w_{1,4}$	0.65
		0.18–0.20	$w_{1,5}$	0.58
		0.20–0.22	$w_{1,6}$	0.52
		0.22–0.24	$w_{1,7}$	0.48
		0.24–0.26	$w_{1,8}$	0.44
		0.26–0.28	$w_{1,9}$	0.41
		0.28–0.30	$w_{1,10}$	0.38
	Land cover (% greenery)	Less than 5%	$w_{2,1}$	1
		5–10%	$w_{2,2}$	0.9
		10–15%	$w_{2,3}$	0.8
		15–20%	$w_{2,4}$	0.7
		20–25%	$w_{2,5}$	0.6
		25–30%	$w_{2,6}$	0.5
		30–35%	$w_{2,7}$	0.4
		35–40%	$w_{2,8}$	0.3
		40–45%	$w_{2,9}$	0.2
		More than 45%	$w_{2,10}$	0.1
Anthropogenic heat	Population density	More than 20,000 ab/km^2	$w_{3,1}$	1
		18,000–20,000 ab/km^2	$w_{3,2}$	0.91
		16,000–18,000 ab/km^2	$w_{3,3}$	0.82
		14,000–16,000 ab/km^2	$w_{3,4}$	0.73
		12,000–14,000 ab/km^2	$w_{3,5}$	0.64
		10,000–12,000 ab/km^2	$w_{3,6}$	0.55
		8,000–10,000 ab/km^2	$w_{3,7}$	0.46
		6,000–8,000 ab/km^2	$w_{3,8}$	0.36
		4,000–6,000 ab/km^2	$w_{3,9}$	0.26
		2,000–4,000 ab/km^2	$w_{3,10}$	0.15
		Less than 2,000 ab/km^2	$w_{3,11}$	0.07

Ud		City	Max UHII
Data for Calibration	1	Adana	9.0
	2	Apeldoorn	6.2
	3	Assen	4.0
	4	Bucharest	5.1
	5	Bursa	7.0
	6	Damwoude	3.2
	7	Delft	4.8
	8	Doornenburg	5.7
	9	Firenze	5.8
	10	Gaziantep	5.0
	11	Glasgow	6.0
	12	Groningen	3.1
	13	Haarlem	5.7
	14	Heemskerk	5.9
	15	Heerhugowaard	6.2
	16	Houten	3.0
	17	IJsselmuiden	6.8
	18	Izmir	7.0
	19	Leeuwarden	3.0
	20	Leiden	5.6
	21	Łódz	7.0
	22	London, City centre	7.6
	23	London, Spitalfields	8.6
	24	Losser	6.8
	25	Madrid	6.0
	26	Moscow, City centre	9.8
	27	Padova	6.0
	28	Paris, City centre	8.0
	29	Paris, Nord	4.6
	30	Purmerend	4.6
	31	Rome, City centre	6.5
	32	Rome, Roma3	4.7
	33	Rotterdam, City centre	7.9
	34	Rotterdam, East	4.8
	35	Rotterdam, South	6.9
	36	Rotterdam, West	9.8
	37	The Hague	5.6
	38	Torino, Consolata	9.0
	39	Trento Molino Vittoria	7.0
	40	Voorburg	5.3
	41	Wageningen	5.6

FIG. 3. UHIIs extracted from a literature review.

investigated urban districts by analyzing an area within 500 m from the relative weather stations. This analysis is carried out by following four steps: (i) construction of the Landsat images and database and exploiting Landsat mission; (ii) adoption of a cloud masking procedure to exclude the cloud pixels from the analysis; (iii) calculation of *greenery*; and (iv) calculation of *albedo*. Note that all the four steps are implemented in GEE environment through JavaScript API.

(i) The first step consists of extract Landsat images of the 41 urban districts. In particular, Landsat mission 5 provides data of 39 urban districts, whereas data regarding the remaining 2 districts are extracted from Landsat mission 8. Table 2 shows for every urban district, the obtained information including Landsat Mission, Acquisition period, Sensor Type, Data ID, and Cloud Cover (%) at the time of acquisition. All collected images are provided in the Universal Transverse Mercator projection and the World Geodetic System (WGS84) datum. In particular, the considered acquisition period for the RS data is consistent with the effective UHII data obtained for the investigated 41 urban districts. The processing phase is implemented directly in the GEE platform speeding up the overall data acquisition procedure (Gorelick *et al.*, 2017). Indeed, in such cloud-based platforms, handling geo-big data, it is possible to download both raw and preprocessed data by drastically reducing the processing time (Kumar and Mutanga, 2018).

(ii) Once the database is constructed, cloud masking procedure is carried out by adopting proper filters suitable for making the clouds transparent and excluding the corresponding pixels during the processing phase. To meet such purpose, the methodology proposed by Mateo-Garcia *et al.* (2018), based on the information provided by the quality assessment band, is applied. No additional orthorectification steps need to be applied because the accuracy provided by the process is considered satisfactory. This implies that the further processing steps (*Greenery* and *Albedo* evaluation) are directly calculated on images resultant from cloud cover masking procedure.

(iii) Green areas percentage (*Greenery*) can be quickly extracted by applying the vegetation indices (VIs) approach. Indeed, as suggested by Anchang *et al.* (2016), it is the most efficient classification method to handle a large volume of geospatial data and to extract *greenery* at large scale. Among the several VIs, the SwirTirRed index (STRed index) (Capolupo *et al.*, 2020a, 2020c) is applied because it is considered one of the most efficient and effective index as demonstrated in Capolupo *et al.* (2020b). STRed index is implemented in GEE environment according to the following Equation (2):

$$\text{STRed index} = \frac{\text{SWIR1} + R - \text{TIR1}}{\text{SWIR1} + R + \text{TIR1}} \tag{2}$$

where SWIR1 is the short wavelength infrared with wavelength in the range 1.57–1.65, R is the red band, and TIR1 is the thermal infrared band.

(iv) The last RS step consists of the albedo evaluation for each urban district. This evaluation is obtained by programming a proper code in the GEE platform and exploiting the following equation proposed by Allen *et al.* (2002) [Eq. (3)]:

$$\text{Albedo} = \frac{(0.356 \times B) + (0.130 \times R) + (0.373 \times \text{NIR}) + (0.085 \times \text{SWIR1}) + (0.072 \times \text{SWIR2}) - 0.018}{1.016} \tag{3}$$

Table 2. Selected Landsat Data Description

UD	Landsat mission	Acquisition period	Sensor type	Data ID	Cloud cover (%)
1	Landsat 5	June 1990	TM	LT05_L1TP_175034_19900610_20180209_01_T1	1
2	Landsat 5	June 2009	TM	LT05_L1TP_197024_20090624_20161024_01_T1	0
3	Landsat 5	September 2008	TM	LT05_L1TP_197023_20080909_20180117_01_T1	5
4	Landsat 5	July 2007	TM	LT05_L1TP_183029_20070719_20161113_01_T1	1
5	Landsat 5	June 1990	TM	LT05_L1TP_180032_19900613_20180210_01_T1	0
6	Landsat 5	September 2008	TM	LT05_L1TP_197023_20080909_20180117_01_T1	5
7	Landsat 5	August 2007	TM	LT05_L1TP_199024_20070804_20180116_01_T1	2
8	Landsat 5	June 2009	TM	LT05_L1TP_197024_20090624_20161024_01_T1	0
9	Landsat 5	June 2002	TM	LT05_L1TP_192030_20020618_20161208_01_T1	0
10	Landsat 5	August 1989	TM	LT05_L1TP_174034_19890819_20180208_01_T1	0
11	Landsat 5	July 2011	TM	LT05_L1TP_205021_20110724_20161008_01_T1	2
12	Landsat 5	September 2008	TM	LT05_L1TP_197023_20080909_20180117_01_T1	5
13	Landsat 5	September 2006	TM	LT05_L1TP_198024_20060911_20161118_01_T1	0
14	Landsat 5	September 2005	TM	LT05_L1TP_198023_20050908_20161124_01_T1	1
15	Landsat 5	September 2006	TM	LT05_L1TP_198024_20060911_20161118_01_T1	0
16	Landsat 5	September 2006	TM	LT05_L1TP_198024_20060911_20161118_01_T1	0
17	Landsat 5	July 2006	TM	LT05_L1TP_198023_20060725_20161120_01_T1	1
18	Landsat 5	July 1990	TM	LT05_L1TP_181033_19900706_20180210_01_T1	0
19	Landsat 5	September 2008	TM	LT05_L1TP_197023_20080909_20180117_01_T1	5
20	Landsat 5	July 2006	TM	LT05_L1TP_199024_20060716_20161120_01_T1	0
21	Landsat 5	July 1994	TM	LT05_L1TP_188024_19940702_20170113_01_T1	0
22	Landsat 5	June 2000	TM	LT05_L1TP_202024_20000618_20171211_01_T1	0
23	Landsat 5	June 2000	TM	LT05_L1TP_202024_20000618_20171211_01_T1	0
24	Landsat 5	July 2006	TM	LT05_L1TP_197024_20060718_20161120_01_T1	0
25	Landsat 5	August 2008	TM	LT05_L1TP_201032_20080820_20180116_01_T1	0
26	Landsat 5	July 2010	TM	LT05_L1TP_178021_20100724_20161014_01_T1	1
27	Landsat 5	June 2011	TM	LT05_L1TP_192028_20110627_20161008_01_T1	5
28	Landsat 5	June 1994	TM	LT05_L1TP_199026_19940613_20180216_01_T1	31
29	Landsat 5	June 1994	TM	LT05_L1TP_199026_19940613_20180216_01_T1	31
30	Landsat 5	April 2008	TM	LT05_L1TP_198023_20080409_20180311_01_T1	7
31	Landsat 8	July 2015	OLI/TIRS	LC08_L1TP_191031_20150717_20170407_01_T1	0.92
32	Landsat 8	July 2015	OLI/TIRS	LC08_L1TP_191031_20150717_20170407_01_T1	0.92
33	Landsat 5	July 2009	TM	LT05_L1TP_198024_20090701_20161025_01_T1	5
34	Landsat 5	June 2010	TM	LT05_L1TP_198024_20100602_20161015_01_T1	4
35	Landsat 5	June 2010	TM	LT05_L1TP_198024_20100602_20161015_01_T1	4
36	Landsat 5	June 2010	TM	LT05_L1TP_198024_20100602_20161015_01_T1	4
37	Landsat 5	August 2007	TM	LT05_L1TP_199024_20070804_20180116_01_T1	2
38	Landsat 5	August 2009	TM	LT05_L1TP_194029_20090822_20161022_01_T1	7
39	Landsat 5	July 2007	TM	LT05_L1TP_193028_20070725_20161112_01_T1	3
40	Landsat 5	August 2007	TM	LT05_L1TP_199024_20070804_20180116_01_T1	2
41	Landsat 5	September 2008	TM	LT05_L1TP_197023_20080909_20180117_01_T1	5

OLI, Operational Land Imager; TIRS, Thermal Infrared Sensors; TM, Thematic Mapper.

where B, R, and NIR are the blue, red, and near infraRed bands, respectively, and SWIR2 is the short wavelength infrared with wavelength in the range 2.11–2.29. In addition, note that Top of Atmosphere corrected bands is used. To sum up, the RS approach is given in Fig. 4.

Anthropogenic heat. The anthropogenic heat is represented by the single criterion ''population density.'' Data regarding the population density can be obtained by exploiting the Eurostat (2018), and integrating some missing data of small Netherland cities by a specific search on local websites. The complete dataset for calibration is given in Supplementary Table S1.

Calibration

In this section, the simplified index is calibrated to enable its application with a refined RS data acquisition. Starting from the index defined in Overview of the Methodological Approach to Achieve the Index section, a mathematical programming (MP) problem is formulated to obtain calibrated weights by an optimization procedure by exploiting the effective UHII data acquired in 41 urban districts.

MP and calibration

To obtain the weights v_i and calibrate the index defined in Equation (1), $K=41$ urban districts ($\mathrm{Ud}=1,\ldots,K$) are considered in eight cities of the European continent. The index of $I^{\mathrm{Ud}}_{\mathrm{RS,\,UHII}}$ associated with the urban districts $\mathrm{Ud}=1,\ldots,K$ is written in function of the column vector of weights $v=[v^1, v^2, v^3]^{\mathrm{T}}$ as follows:

$$I^{\mathrm{Ud}}_{\mathrm{RS,\,UHII}}(\boldsymbol{v}) = v_1 \times w_{1j} + v_2 \times w_{2j} + v_3 \times w_{3j} \qquad (4)$$

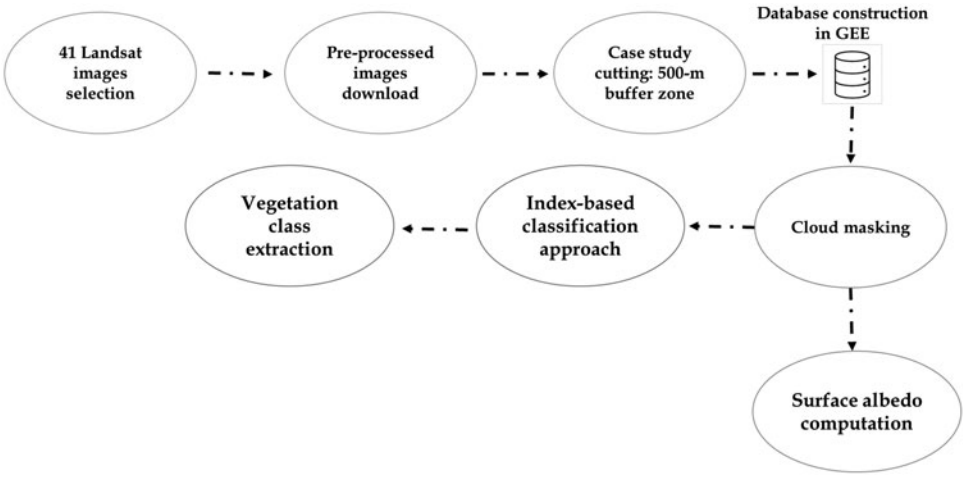

FIG. 4. Flowchart of RS approach. GEE, Google Earth Engine; RS, remote sensing.

where j are the alternatives associated with the Ud-th urban district.

Subsequently, it is possible to define the function $F(\boldsymbol{v})$, which evaluates the difference between the values of $I_{\text{UHII}}^{\text{Ud}}$ and the effective max UHII^{Ud} reported in Fig. 3 calculated for each examined urban districts $\text{Ud} = 1,\ldots,K$:

$$F(\boldsymbol{v}) = \sum_{\text{Ud}=1}^{K} \left(I_{\text{RS, UHII}}^{\text{Ud}}(\boldsymbol{v}) - \text{UHII}^{\text{Ud}}\right)^2 \tag{5}$$

To calibrate vector $\boldsymbol{v}$, it is assumed that the index of potential $I_{\text{RS, UHII}}^{\text{Ud}}$ should be as close as possible to the index of effective max UHII^{Ud} for the considered urban districts.

$F(\boldsymbol{v})$ represents the sum of the differences between the proposed index and the effective intensity of the registered phenomenon. Consequently, $F(\boldsymbol{v})$ is set as the objective function to be minimized by satisfying a set of constraints on vector $\boldsymbol{v}$:

$$\Gamma(\boldsymbol{v}) : v_i \geq 0 \text{ for } i = 1, \cdots, 3 \tag{6}$$

Constraints [Equations (7) and (8)] are set to avoid negative or null values of the weights.

Now, to calculate vector $\boldsymbol{v}$, the following MP problem is formulated:

$$\min F(\boldsymbol{v}) \tag{7}$$

$$\text{subject to } \Gamma(\boldsymbol{v}) \tag{8}$$

Calibration results

A generalized reduced gradient method (Lasdon *et al.*, 1974) is applied to solve the MP problem by using a multistart of a population of 1,000 and a convergence of 0.001. The MP solution outcomes the calibrated weights given in Fig. 5. In addition, the results of the calibration of the simplified index (working with RS data acquisition: *satellite image analysis approach*) is compared with the calibration of the *approach of Sangiorgio et al. (2020)*. In particular, Fig. 5 in the left part shows a pie chart regarding the influence of every criterion (or parameters) expressed in percentage calibrated by using RS data (*satellite image analysis approach*) and in the right the pie chart regarding the calibration of Sangiorgio *et al.* (2020). Note that the

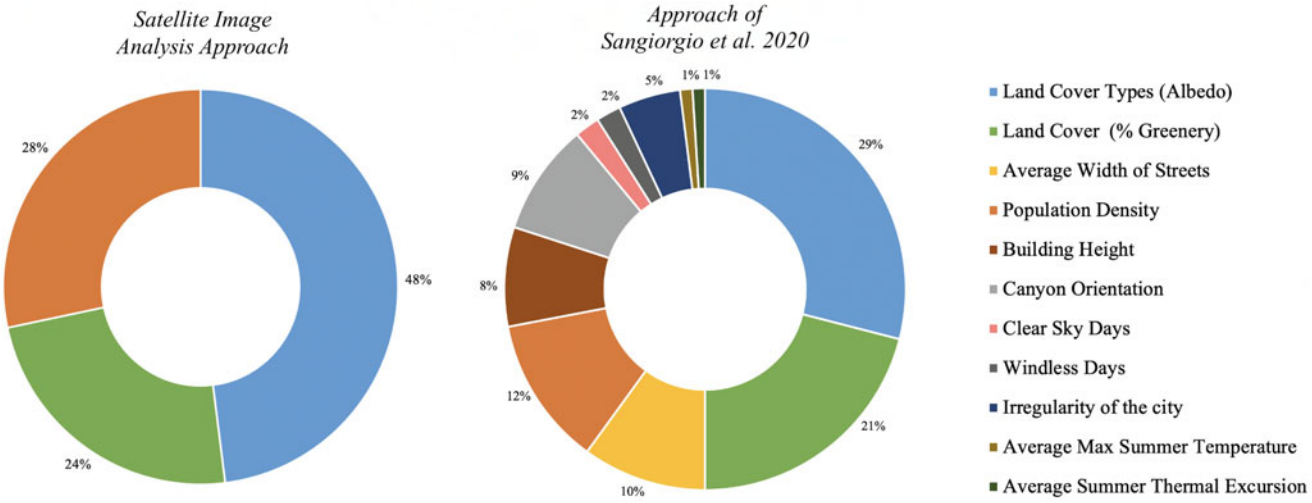

FIG. 5. Calibrated weights, influence of each parameter in the UHII and comparison with an existing multiparametric approach of Sangiorgio *et al.* (2020).

simplified approach is achieved by involving the three most important parameters of the approach of Sangiorgio *et al.* (2020).

Absolute and relative error

To explicitly validate the proposed calibration, a second analysis is performed to identify the *Absolute Error* and the *Mean Relative Error* of the proposed index in comparison with the approach of Sangiorgio *et al.* (2020). In particular, the values obtained with index $I_{RS,UHII}$ is compared with the effective absolute max UHII obtained from the bibliography (RS data acquisition methods and Sangiorgio *et al.*, 2020). To this aim, a Jackknife approach is used to perform a resampling of the input data and verify both the reliability and the robustness of the index by displaying statistical graphs. In particular, a one-by-one removal of the 41 urban districts is performed and every removal the MP problem is solved to verify that the solution does not change significantly.

Figure 6 shows the statistical graph (boxplot) of the *Absolute Error* and *Mean Relative Error* obtained for the two approaches. More in detail, the boxes represent the distribution of the error (°C for the *Absolute Error* and % for the *Relative Error*) and the black horizontal line inside the boxes denotes the median of the sample. Although the box contains all results within the 25th and 75th percentile of the population, the vertical line contains all results that are not considered outliers. The *Mean Relative Error* is represented in the same graph by the symbol "×."

This additional analysis demonstrates that the proposed index is able to quantify the potential absolute max UHII with an average accuracy of ∼1.2°C (mean absolute error <1.2°C). In addition, in >70% of the investigated urban district the relative error is <10%. On the contrary, in the urban district where the absolute max UHII is small, often there is a higher error (>15%) even if the absolute error remains ∼1°C. The mean relative error is ∼20% and 15% for the simplified index and Sangiorgio's approach, respectively. The proposed approach provides accuracy only slightly lower but ensures greater ease of use and applicability.

In addition, such error and can be considered acceptable to the effective application of the proposed index as it is similar to the reliability that characterizes the UHII measurements with standard fixed station. Indeed, the conventional approach to measure UHII can be affected by an inaccuracy owing to the choice of the rural station measurement to be compared with the city station measurement as discussed by Oke (1991).

Application and Comparison

To verify the effectiveness of the proposed approach, the index is applied to the case study of Berlin. Moreover, a comparison of the two different approaches is performed to show the differences of the two methods.

The index application: the case of Berlin

The resulting indexes are able to forecast the absolute max UHII in the urban districts by using the input data including characteristics of the city (in terms of *albedo* and *greenery*) and *anthropogenic heat*.

To provide an example, there are no exhaustive studies on the heat island effect for the whole city of Berlin in related literature. To this reason, the proposed index can be very useful to study the magnitude of the phenomenon in the city exploiting an RS data analysis.

The collection procedure allows to easily achieve the input data of all the 96 urban districts of the city of Berlin as given in Supplementary Tables S2 and S3. Note that, data are acquired by considering an area within 500 m centroid of considered districts. In addition, Supplementary Tables S2 and S3 show the two datasets regarding the districts of Berlin, one obtained with the procedure of Sangiorgio *et al.* (2020) and one with the proposed RS procedure, respectively. Note that the RS procedure is applied with both the data of Landsat 5, acquired on July 2, 2011 and Landsat 8, taken on June 24, 2019, to identify any differences in the applicability of the

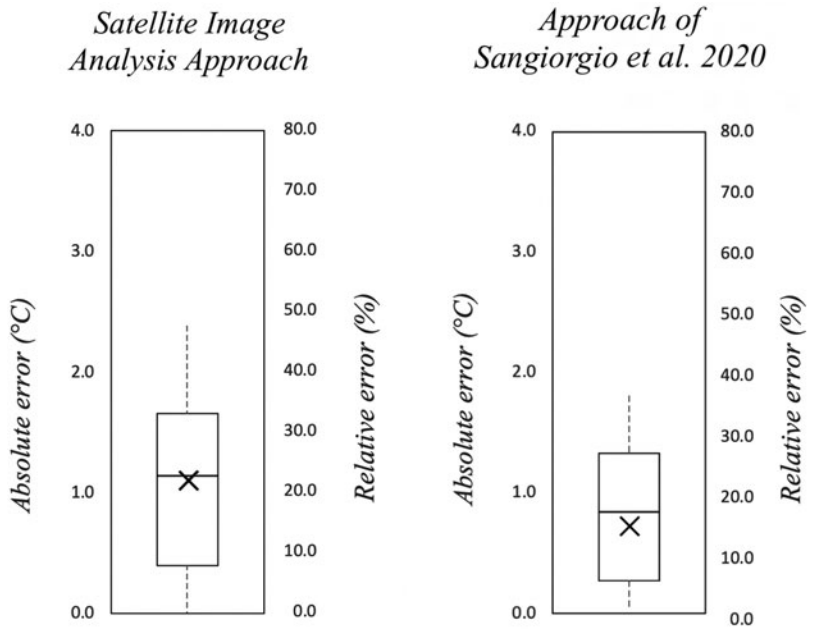

FIG. 6. Boxplot of the absolute error and mean relative error obtained for the two approaches.

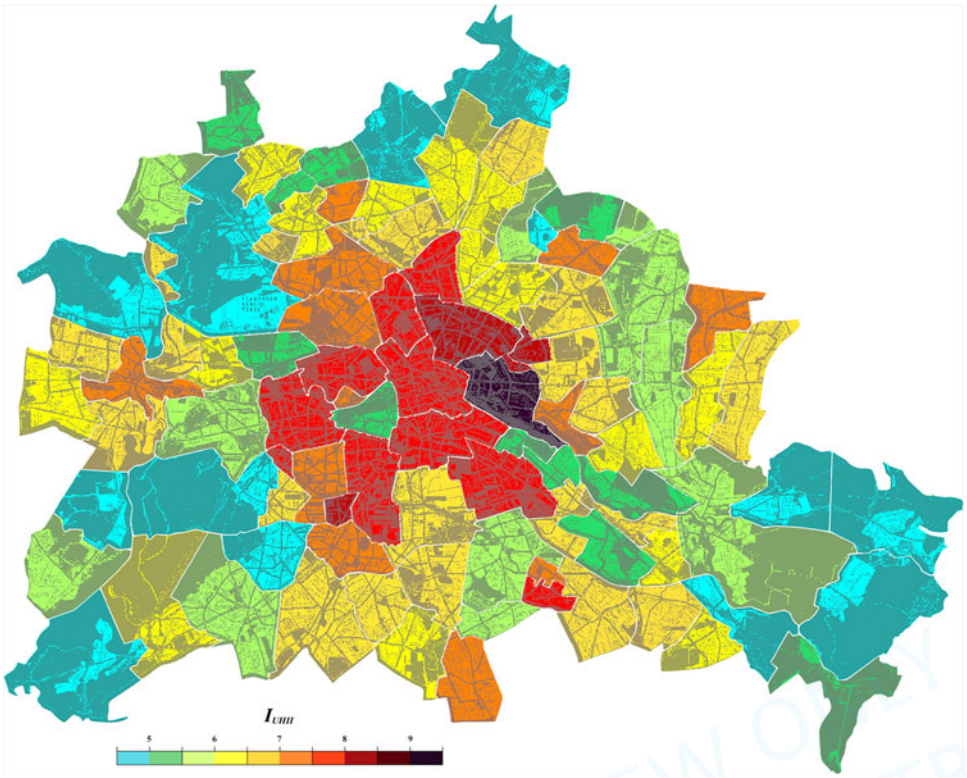

FIG. 7. Example of the application of the $I_{RS,UHII}$ (RS data from Landsat 8) to create an intensity map of the city districts of Berlin.

method with the different satellites (comparison described in the next subsection).

Figure 7 shows the application of the proposed index (exploiting data from Landsat 8) to generate an intensity map (and show the magnitude of the phenomenon) of the city of Berlin for the Absolute Max UHII. The central areas of Berlin (urban districts of Mitte or Friedrichshain) are the most subject to suffer the UHI caused by an intensely developed urban fabric. The only few exceptions, as an example, the urban district of Hellersdorf may be subject to high-absolute max UHII because of the high housing density and lower presence of green. On the contrary, in most districts of Berlin, there is lot of greenery between parks and urban woods that are able to mitigate the effects of the phenomenon. These results are in line with the study of Menberg *et al.* (2013) that investigates the distribution of the surface air temperature in Berlin.

The comparison of different approaches

To show the differences of the two approaches and investigate the contribution of diverse satellite data, the intensity map of Berlin is evaluated by the index applied with: (1) the *approach of Sangiorgio et al. (2020)*; (2) the simplified index exploiting *satellite image analysis approach* using Landsat 5; (3) and the simplified index exploiting *satellite image analysis approach* using Landsat 8. Figure 8 shows the different intensity maps obtained with the two approaches and the three different datasets.

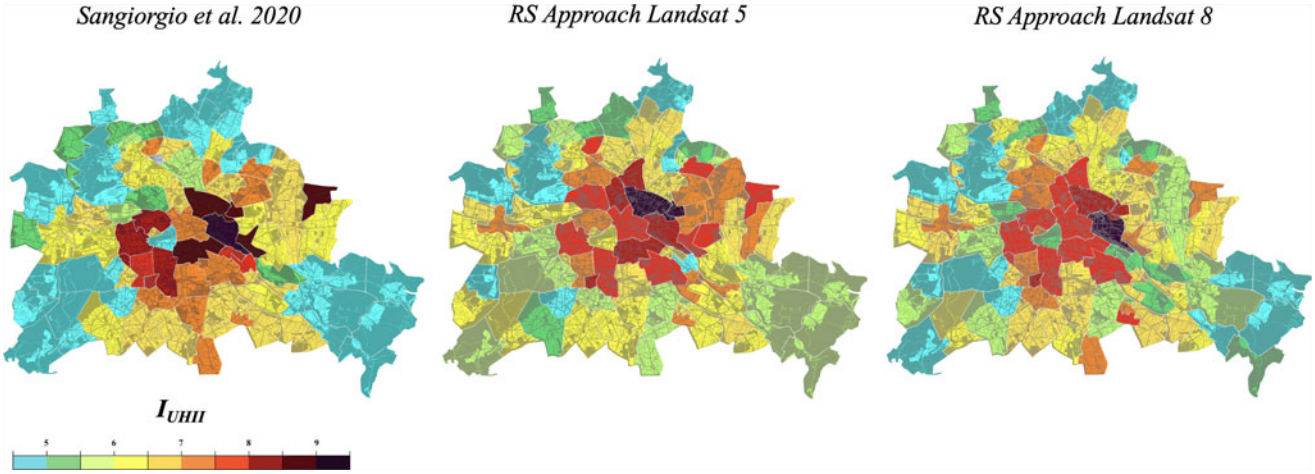

FIG. 8. Example of the application of the $I_{RS,UHII}$ and comparison with Sangiorgio *et al*. (2020), Landsat 5, and Landsat 8 to create a intensity map of the city districts of Berlin.

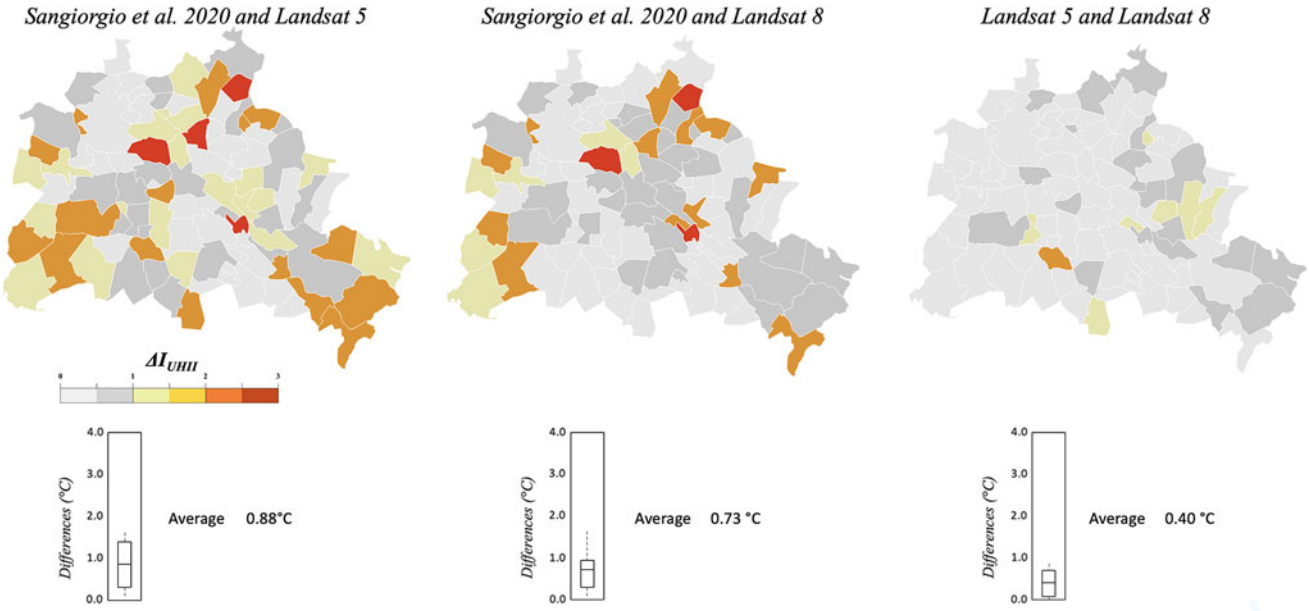

FIG. 9. Pair comparisons of the intensity maps of Berlin and boxplot of the Δ_{UHII} evaluated for every urban district.

Moreover, Fig. 9 emphasizes the differences of the various intensity maps showing pair comparisons of the three maps obtained. For every pair comparison, a boxplot representing the differences of the estimated absolute max UHII for all the city urban districts Δ_{UHII} is given.

The *approach of Sangiorgio et al. (2020)* allows achieving good results for the estimation of both the high- and low-absolute max UHII. On the contrary, this approach is time consuming and involves a large number of parameters in comparison with the simplified RS approach.

The *satellite image analysis approach* using Landsat 5 is accurate for districts with medium and high UHII but provides a slight overestimation of the districts with low UHII.

On the contrary, Landsat 8 is very accurate for districts with low UHII and slightly underestimates districts with high UHII.

However, the average differences among the three approaches are far below 1°C, confirming that both the approaches and the three data acquisition methods are effective. Specifically, such an outcome provides relevant contribution in detecting the UHI in specific historical periods, owing to the reliability of Landsat data (in both the considered missions 5 and 8). Indeed, Landsat is the only satellite platform providing free continuous information from 1973. Thus, the Landsat-based RS approach allows extracting information in a specific temporal period. Consequently, by using this approach it is possible to carry out multi-temporal analysis suitable for investigating UHI evolution over the time.

Conclusions

The proposed work presents a simplified index that allows to evaluate the potential absolute max UHII in urban districts by exploiting satellite image analysis to identify the *albedo*, *greenery*, and *population density*.

The novelty of the proposed approach is twofold.

First, in comparison with previous approaches, such as the index of Sangiorgio *et al.* (2020), the proposed method is simplified, automated, and applicable at a large scale. Indeed, the proposed index can exploit a structured RS evaluation to acquire *albedo* and *greenery* with a cloud-based platform handling geo-big data at large scale. The integration of such data acquisition approach in the index provides the great advantage of processing the big data by using in parallel 100 processors, speeding up the overall data acquisition procedure.

Second, the RS-based procedure provides relevant contribution in detecting the UHI in specific historical periods owing to the reliability of Landsat providing free continuous information from 1973. Thus, the Landsat-based RS approach allows extracting information in a specific temporal period and simultaneously carrying out multi-temporal analysis suitable for investigating UHI evolution over the time.

The proposed index could be a useful tool to quantify the potential UHII in any phase of an urban development, from the project phase to the construction maintenance and management phases. The index could also be used to evaluate local mitigation strategies and the effectiveness of retrofit interventions to improve the energy performances of buildings. Beyond this, researchers can also use this index to obtain maps of intensity at different scales: urban, regional, and national.

Future research will evaluate the vulnerability index and exposure index to the UHII phenomenon to obtain an overall risk index of the phenomenon. In addition, the proposed index will be integrated in Spatial Decision Support Systems for the large-scale risk assessment useful to set effective mitigation strategies.

Authors' Contributions

Conceptualization: V.S., F.F., and M.S.; methodology: V.S. and A.C.; validation, V.S.; formal analysis: V.S. and A.C.; data curation: V.S. and A.C.; writing—original draft preparation: V.S.; writing—review and editing: V.S., F.F., E.T., and M.S.; visualization: V.S.; supervision: F.F., E.T., and M.S. All authors have read and agreed to the published version of the article.

Author Disclosure Statement

No competing financial interests exist.

Funding Information

No funding was received for this article. The funders had no role in the design of the study; in the collection, analyses, or interpretation of data; in the writing of the article, or in the decision to publish the results.

Supplementary Material

Supplementary Table S1
Supplementary Table S2
Supplementary Table S3

References

Al-Ghussain, L. (2019). Global warming: Review on driving forces and mitigation. *Environ. Prog. Sustain Energy* 38, 13.

Allen, R.G., Tasumi, M., Trezza, R., Waters, R., and Bastiaanssen, W. (2002). *SEBAL Surface Energy Balance Algorithms for Land—Advanced Training and Users Manual—Idaho Implementation (Version 1.0)*. Boise, ID: The Idaho Department of Water Resources.

Anchang, J.Y., Ananga, E.O., and Pu, R. (2016). An efficient unsupervised index based approach for mapping urban vegetation from IKONOS imagery. *Int. J. Appl. Earth Obs. Geoinf.* 50, 211.

Apollonio, C., Balacco, G., Novelli, A., Tarantino, E., and Piccinni, A.F. (2016). Land use change impact on flooding areas: The case study of Cervaro Basin (Italy). *Sustainability* 8, 996.

Boccia, L., Capolupo, A., Rigillo, M., and Russo, V.T. (2020). Abandonment hazards in a Mediterranean cultural landscape. *J. Hazard Toxic Radioact. Waste* 24, 04019034.

Busato, F., Lazzarin, R.M., and Noro, M. (2014). Three years of study of the Urban Heat Island in Padua: Experimental results. *Sustain Cities Soc.* 10, 251.

Cantelli, A. Monti, P., and Leuzzi, G. (2015). Numerical study of the urban geometrical representation impact in a surface energy budget model. *Environ. Fluid Mech.* 1525, 1.

Capolupo, A., Kooistra, L., and Boccia, L. (2018). A novel approach for detecting agricultural terraced landscapes from historical and contemporaneous photogrammetric aerial photos. *Int. J. Appl. Earth Obs. Geoinf.* 73, 800.

Capolupo, A., Monterisi, C., Caporusso, G., and Tarantino, E. (2020a). Extracting land cover data using GEE: A review of the classification indices. In *International Conference on Computational Science and Its Applications*. Springer, Cham, p. 782–796.

Capolupo, A., Monterisi, C., Saponaro, M., and Tarantino, E. (2020b). Multi-temporal analysis of land cover changes using Landsat data through Google Earth Engine platform. In *Eighth International Conference on Remote Sensing and Geoinformation of the Environment (RSCy2020)*, Vol. 11524. Bellingham, Washington: International Society for Optics and Photonics, p. 1152419.

Capolupo, A., Monterisi, C., and Tarantino, E. (2020c). Landsat Images Classification Algorithm (LICA) to automatically extract land cover information in google earth engine environment. *Remote Sens.* 12, 1201.

Caprioli, M., and Tarantino, E. (2001). Accuracy assessment of per-field classification integrating very fine spatial resolution satellite imagery with topographic data. *J. Geospat. Eng.* 3, 127.

Chen, X.L., Zhao, H.M., Li, P.X., and Yin, Z.Y. (2006). Remote sensing image-based analysis of the relationship between urban heat island and land use/cover changes. *Remote Sens. Environ.* 104, 133.

Cheval, S., Dumitrescu, A., and Bell, A. (2009). The urban heat island of Bucharest during the extreme high temperatures of July 2007. *Theor. Appl. Climatol.* 97, 391.

Eurostat-Europeanstatistics. (2018). Population density. Available at: https://ec.europa.eu/info/departments/eurostat-european-statistics (accessed January 20, 2020).

Fortuniak, K., Kłysik, K., and Wibig, J. (2006). Urban–rural contrasts of meteorological parameters in Łódź. *Theor. Appl. Climatol.* 84, 91.

Giovannini, L., Zardi, D., and De Franceschi, M. (2011). Analysis of the urban thermal fingerprint of the city of Trento in the Alps. *J. Appl. Meteorol. Climatol.* 50, 1145.

Gorelick, N., Hancher, M., Dixon, M., Ilyushchenko, S., Thau, D., and Moore, R. (2017). Google Earth Engine: Planetary-scale geospatial analysis for everyone. *Remote Sens. Environ.* 202, 18.

Guattari, C., Evangelisti, L., and Balaras, C.A. (2018). On the assessment of urban heat island phenomenon and its effects on building energy performance: A case study of Rome (Italy). *Energy Build.* 158, 605.

Heaviside, C., Vardoulakis, S., and Cai, X.M. (2016). Attribution of mortality to the urban heat island during heatwaves in the West Midlands, UK. *Environ. Health* 15, 49.

Kolokotroni, M., and Giridharan, R. (2008). Urban heat island intensity in London: An investigation of the impact of physical characteristics on changes in outdoor air temperature during summer. *Sol. Energy.* 82, 986.

Krüger, E., and Emmanuel, R. (2013). Accounting for atmospheric stability conditions in urban heat island studies: The case of Glasgow, UK. *Landsc. Urban Plan.* 117, 112.

Kumar, L., and Mutanga, O. (2018). Google Earth Engine applications since inception: Usage, trends, and potential. *Remote Sens.* 10, 1509.

Lasdon, L.S., Fox, R.L., and Ratner, M.W. (1974). Nonlinear optimization using the generalized reduced gradient method. *Revue française d'automatique, informatique, recherche opérationnelle. Rev Fr Inform Rech O*. 8(V3), 73.

Lemonsu, A., and Masson, V. (2002). Simulation of a summer urban breeze over Paris. *Boundary Layer Meteorol.* 104, 463.

Marando, F., Salvatori, E., Sebastiani, A., Fusaro, L., and Manes, F. (2019). Regulating ecosystem services and green infrastructure: Assessment of urban heat island effect mitigation in the municipality of Rome, Italy. *Ecol. Modell.* 392, 92.

Mateo-García, G., Gómez-Chova, L., Amorós-López, J., Muñoz-Marí, J., and Camps-Valls, G. (2018). Multitemporal cloud masking in the Google Earth Engine. *Remote Sens.* 10, p.1079.

McMichael, A.J., Woodruff, R.E., and Hales, S. (2006). Climate change and human health: Present and future risks. *Lancet* 367, 859.

Menberg, K., Bayer, P., Zosseder, K., Rumohr, S., and Blum, P. (2013). Subsurface urban heat islands in German cities. *Sci. Total Environ*. 442, 123.

Merkin, R. (2004). *The Urban Heat Island's Effect on the Diurnal Temperature Range*. Doctoral Dissertation, Massachusetts Institute of Technology.

Milelli, M. (2016). Urban heat island effects over Torino. *COSMO Newsl*. 16, 1.

Mirzaei, M., Verrelst, J., Arbabi, M., Shaklabadi, Z., and Lotfizadeh, M. (2020). Urban heat island monitoring and impacts on Citizen's General Health Status in Isfahan Metropolis: A remote sensing and field survey approach. *Remote Sens.* 12, 1350.

Oke, T.R. (1991). Climate of cities. In *Climate in Human Perspective*. Dordrecht: Springer, pp. 61–75. [Epub ahead of print]; DOI: 10.1007/978-94-011-3320-3_6

Oke, T.R., Mills, G., Christen, A., and Voogt, J.A. (2017). *Urban climates.* Cambridge, UK: Cambridge University Press.

Pantavou, K., Theoharatos, G., Mavrakis, A., and Santamouris, M. (2011). Evaluating thermal comfort conditions and health responses during an extremely hot summer in Athens. *Build. Environ.* 46, 339.

Petralli, M., Prokopp, A., Morabito, M., Bartolini, G., Torrigiani, T., and Orlandini, S. (2006). Ruolo delle aree verdi nella mitigazione dell'isola di calore urbana: Uno studio nella città di Firenze. *Riv. Ital. Agrometeorol.* 1, 51.

Sangiorgio, V., Fiorito, F., and Santamouris, M. (2020). Development of a holistic urban heat island evaluation methodology. *Sci. Rep.* 10, 1.

Sangiorgio, V., and Parisi, F. (2020). A multicriteria approach for risk assessment of Covid-19 in urban district lockdown. *Saf. Sci.* 104862.

Sangiorgio, V., Uva, G., Fatiguso, F., and Adam, J.M. (2019). A new index to evaluate exposure and potential damage to RC building structures in coastal areas. *Eng. Fail. Anal.* 100, 439.

Santamouris, M. (2015). Analyzing the heat island magnitude and characteristics in one hundred Asian and Australian cities and regions. *Sci. Total Environ.* 512, 582.

Santamouris, M. (2016). Innovating to zero the building sector in Europe: Minimising the energy consumption, eradication of the energy poverty and mitigating the local climate change. *Sol. Energy*. 128, 61.

Santamouris, M. (2020). Recent progress on urban overheating and heat island research. Integrated assessment of the energy, environmental, vulnerability and health impact. Synergies with the global climate change. *Energy Build.* 207, 109482.

Sarzana, T., Maltese, A., Capolupo, A., and Tarantino, E. (2020). July. Post-processing of pixel and object-based land cover classifications of very high spatial resolution images. In *International Conference on Computational Science and Its Applications*. Cham: Springer, p. 797.

Singh, A., and Purohit, B.M. (2014). Public health impacts of global warming and climate change. *Peace Rev*. 26, 112.

Sociedad Limitada. Tutiempo Network (2020). Climate data: Europe. Available at: https://www.tutiempo.net (accessed March 30, 2020).

Tarantino, E., and Figorito, B. (2012). Mapping rural areas with widespread plastic covered vineyards using true color aerial data. *Remote Sens.* 4, 1913.

Tayanc, M., and Toros, H. (1997). Urbanization effects on regional climate change in the case of four large cities of Turkey. *Clim. Change* 35, 501.

Van Hove, L.W.A., Steeneveld, G.J., Jacobs, C.M.J., Heusinkveld, B.G., Elbers, J.A., Moors, E.J., and Holtslag, A.A.M. (2011). Exploring the urban heat island intensity of Dutch cities: assessment based on a literature review, recent meteorological observation and datasets provide by hobby meteorologists (No. 2170). Alterra.

Varentsov, M., Wouters, H., Platonov, V., and Konstantinov, P. (2018). Megacity-induced mesoclimatic effects in the lower atmosphere: A modeling study for multiple summers over Moscow, Russia. *Atmosphere* 9, 50.

Wang, G., Jiang, W., and Wei, M. (2008). An Assessment of Urban Heat Island Effect using Remote Sensing Data. *Mar. Sci. Bull.* 10, 14.

Weng, Q., Lu, D., and Schubring, J. (2004). Estimation of land surface temperature–vegetation abundance relationship for urban heat island studies. *Remote Sens. Environ.* 89, 467.